Laser welding of niobium to AISI 304 steel using a copper interlayer

Jian Zhao[a, e], Mingxiao Shi [b, c, *], Yanjun Li [c], Xiang Ma [d], Zhenxing Fan [a], Hua Yan [a, e]

[a] *College of Materials Engineering, Shanghai University of Engineering Science, Shanghai, China*
[b] *School of Materials Science and Engineering, Jiangsu University of Science and Technology, Zhenjiang, China*
[c] *Department of Materials Science and Engineering, Norwegian University of Science and Technology, Trondheim, Norway*
[d] *Department of Industrial Process Technology, SINTEF Materials and Chemistry, Oslo, Norway*
[e] *Shanghai Collaborative Innovation Center of Laser Advanced Manufacturing Technology, Shanghai, China*

ABSTRACT

Cu interlayers with thicknesses of 1, 1.5, and 2 mm were used to join niobium and AISI 304 steel. Fractures occurred in the weld, the Nb base metal, and the unmelted Cu interlayer when the Cu interlayer thickness was 1, 1.5, and 2 mm, respectively. When the thickness of the Cu interlayer was 1 mm, the weld microstructure consisted of austenite with Cu-rich particles along the austenitic grain boundaries and within the austenitic grains, a composite-like structure (the Fe_2Nb lamellae and particles in a γ matrix) embedded with coarse Cu globules, and a mixture of bulk Fe_7Nb_6, Nb-rich dendrites, and Cu matrix. The bulk brittle Fe_7Nb_6 phase embrittled the joint. However, when the thickness of the Cu interlayer was 1.5 mm, the weld microstructure consisted of austenite with Cu-rich precipitates along the austenitic grain boundaries and a Cu-rich phase embedded with Nb-rich particles and dendrites. Solid-solution strengthening of Cu by Fe was responsible for the improved mechanical properties of the joint. The mixture of Nb-rich particles and dendrites in the Cu matrix was also helpful in enhancing the joint strength. Furthermore, when the thickness of the Cu interlayer was 2 mm, the weld microstructure consisted of austenite with Cu-rich precipitates along the austenitic grain boundaries and within the austenitic grains, an unmelted Cu interlayer, and Nb-rich particles and dendrites embedded in a Cu matrix. The unmelted Cu interlayer reduced the joint strength.

KEYWORDS

laser welding, niobium, AISI 304 steel, microstructure, joint strength

* Corresponding author.
E-mail address: smx@just.edu.cn (M.X. Shi).
Tel.: +86 15005281805.

1. Introduction

The joining of Nb to austenitic stainless steel requires the use of a particle accelerator [1-3]. During the operation of a particle accelerator, the cooling of superconducting Nb by liquid He is accommodated by an austenitic stainless steel container [1]. Therefore, a reliable and cryogenic leak-tight seal is necessary between the Nb cavity and the austenitic stainless steel container. However, the extensive differences in the physical and chemical properties between Nb and stainless steel have caused many problems in their direct joining [3]. The most obvious result is the formation of brittle intermetallics (i.e., Fe_2Nb and Fe_7Nb_6) attributable to the crystallographic mismatch between Nb and stainless steel, which could lead to solidification cracks in the joint and therefore brittle failure [1,3]. Existing solid-state welding methods such as brazing-welding and friction stir welding can inhibit the formation of some intermetallic compounds, so these techniques have become the most common welding methods for joining Nb to dissimilar metals. Alternatively, as reported by Jiao et al. [4] and Taran et al. [5], high-strength welded joints were obtained by explosive welding, however, this approach is scarcely utilized for components with complex geometric shapes. Budkin et al. [6] used electron beam welding-brazing to join 12Cr18Ni10Ti steel to Nb, and the formation probability of metal brittle compounds was decreased by controlling the temperature field of the weld zone. Li et al. [7] studied the electron beam welding-brazing of Nb-1Zr alloy and AISI 304 steel, and brittle metal Fe_2Nb was found at the joint. As evidenced by the above literature, the use of welding-brazing can suppress but not eliminate the formation of intermetallics. Moreover, the strength of the formed joint is weakened by the presence of brittle metal compounds. Nb-1Zr alloy and 1Cr18Ni9Ti steel using a Ni-based solder (BNi-2, BNi-5, and BNi-7) were joined through high-temperature vacuum brazing, and the brazed joint exhibited excellent airtightness and good thermal shock resistance [8]. Kumar et al. [1] studied the vacuum brazing of Nb-AlSI 316L steel with a Ag-28% Cu filler metal; at

the temperature of liquid He, the brazed joint displayed improved hermeticity. An improved vacuum brazing method was developed by Fuerst et al. [2], and a good cryogenic leak-tight joint was obtained via vacuum brazing Nb to stainless steel using a Cu filler metal. Nevertheless, although the formation of brittle intermetallics could be avoided by using an appropriate solder, the problem of low joint strength was not resolved. Notably, some scholars have used electron beam welding to join Nb-1Zr and 321 stainless steel [9,10]. However, brittle metal Fe-Nb was also present, which means that the discrepancies in the mechanical properties and weldability at the joint cannot be avoided in this approach.

Recently, as an alternative advanced welding technique [11], laser welding has received considerable attention for the flexible joining of Nb to stainless steel. Shi et al. [12] offset the laser beam into AISI 304 steel to join the steel to Nb; however, the welding joint was excessively low due to the formation of Fe-Nb intermetallics. Obviously, the addition of an acceptable interlayer featuring good metallurgical compatibility with the two base metals would be a workable technique. In other words, the above-mentioned method is optimal for the laser welding of Nb to AISI 304 steel. Accordingly, Baghjari et al. [3] researched the use of a Ni interlayer for the laser welding of 410 steel-Nb joints and showed that this technique inhibits the formation of Fe-Nb intermetallics and thus could be successfully utilized to join steel and Nb. The most important factor for choosing the interlayer material was its inability to form metal compounds with the base metal. With this criterion in mind, since Cu cannot form intermetallics with either base metal according to the binary Cu-Nb and Fe-Cu phase diagrams given by Massalski et al. [13], Cu was identified as a potential interlayer material for the dissimilar joining of Nb and AISI 304 steel.

In our research, a high-strength AISI 304 steel-Nb joint was obtained by adding a Cu interlayer with a double-pass laser-welding process. Furthermore, the effects of the Cu interlayer thickness on the microstructure and mechanical properties of the joint were studied. This research reveals a pathway for the future development and application of AISI 304 steel-

Nb welding structures.

2. Materials and methods

Annealed commercially pure Nb and austenitic AISI 304 stainless steel were employed as the base metals in this work. The commercially pure Cu for the interlayer material was annealed before the experiment. As described in our previously published article [14], the microstructure of AISI 304 steel consisted of austenitic equiaxed grains with twinning in the grain interiors, and the pure Nb was composed of equiaxed Nb grains, as shown in Fig. 1a and b, respectively. The two base metals, AISI 304 steel and pure Nb, were cut to dimensions of 50×50×2 mm, while the Cu interlayers were designed with a length of 30 mm, a width of 10 mm and three thicknesses: 1 mm, 1.5 mm, and 3 mm. Before welding, the surfaces of these three materials were ground with 180 grit SiC abrasive paper to remove surface oxides and then cleaned by an ultrasonic bath using acetone as a solvent to remove oil and grease.

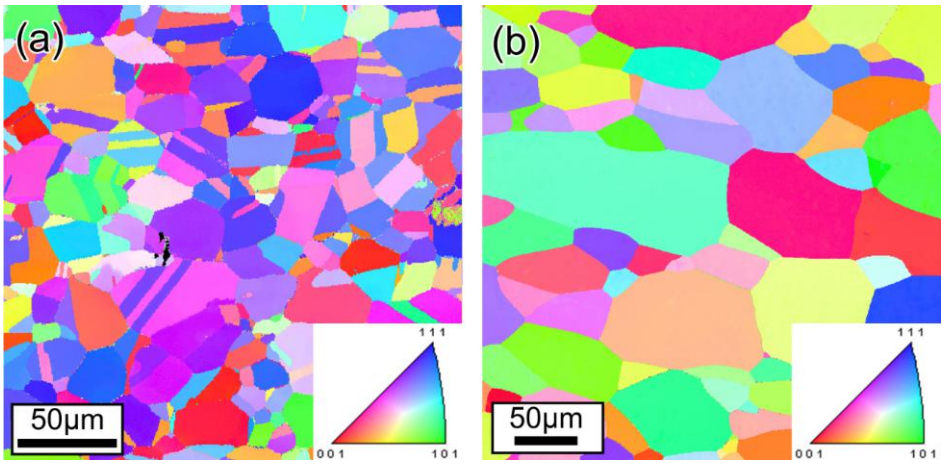

Fig. 1. EBSD inverse pole figure maps of (a) AISI 304 steel and (b) Nb.

A continuous-wave IPG Photonics® YLS-6000-S2-TR ytterbium fiber laser was used in this study. The laser beam with wavelengths of 1065-1080 nm was generated by the fiber laser with a maximum power of 6 kW and was transmitted to a HIGHYAG® BIMO laser processing head through a 200-μm core diameter processing fiber, and the beam was focused by a focusing lens with a 310-mm focal length to obtain a spot diameter of 350 μm. The laser processing head was mounted on an ABB® six-axis robot, which moved the laser processing

head while the weldment remained stationary during welding.

The experiments were carried out in a butt joint configuration with the Cu interlayer embedded between the steel plate and the Nb plate. To achieve the fusion joining of Cu-steel and Cu-Nb, a double-pass laser-welding process was used. The first laser beam was centered on the faying surface between steel and Cu, and the second laser beam was centered on the faying surface between Nb and Cu. The welding parameters employed in the study were as follows: the first laser beam had a laser power of 2 kW, a welding speed of 25 mm/s, and a defocus distance of 0 mm; the second laser beam had a laser power of 2 kW, a welding speed of 30 mm/s, and a defocus distance of 0 mm. Pure argon gas at a flow rate of 15 L/min was used to protect the weldment against oxidation during welding.

After laser welding, the cross sections of the welded joints were cut and then mounted in epoxy resin for further grinding and polishing. Samples for metallographic observation were mechanically ground and polished. Chemical etching of samples was performed with a two-step combination of etchants: the samples were first etched for 4-5 s in a solution of 4 g $CuSO_4 \cdot 5\ H_2O$ + 20 mL HCl + 20 mL H_2O and then etched for 60 s in a solution of 2 g $Fe(NO_3)_3 \cdot 9\ H_2O$ + 50 mL ethanol. The formulations of the etchants were obtained from Han and Zhang [15]. Samples for electron backscatter diffraction (EBSD) analysis were mechanically ground and polished and then vibratory polished with an amplitude of 50% for 70 h.

Metallographic observations of the joints were performed using a VHX-900 optical microscope (OM) and a Zeiss Ultra 55 LE scanning electron microscope (SEM). EBSD analysis of the joints was conducted using a Nordif EBSD detector. The chemical compositions of the different phases of the joints were analyzed by an XFlash® 4010 energy dispersive spectroscopy (EDS) detector.

Tensile specimens with a gauge length of 25 mm based on the GBT 228-2002 standard were cut transversely from the weldments. Tensile tests were carried out at room temperature

with a strain rate of 1.3×10^{-3} s^{-1}. The fracture surfaces were observed by SEM. The Vickers microhardness was determined with a load of 0.1 kg and a dwell time of 10 s. The microhardness profiles were obtained in the horizontal direction of the cross section of the joint.

3. Results and discussion

3.1. Microstructural features of the joints

3.1.1. Joint with a 1-mm-thick Cu interlayer

A cross-sectional macrograph of the joint is shown in Fig. 2a. An asymmetric weld, which is a typical feature of dissimilar metal welds, was observed. As reported by Torkamany et al. [16], the significant differences in the melting points and thermal conductivities between AISI 304 steel and Nb were the main cause of the asymmetric weld shape. Furthermore, two distinct regions, termed zones A and B, were discovered in the weld.

Fig. 2b-d depicts micrographs of zone A. As seen in Fig. 2c and d, precipitates were present along the grain boundaries and within the grains. EDS analyses of the different phases of the joint were carried out, and the results are shown in Table 1. The EDS analyses confirmed that the microstructure of zone A consisted of austenite (γ) and contained some Cu (areas 1-3 in Table 1 and Fig. 2d) and Cu-rich precipitates in the γ matrix (areas 4-7 in Table 1 and Fig. 2d). A similar microstructure was previously observed by Magnabosco et al. [17] in an electron beam-welded austenitic stainless steel-Cu joint. During the irradiation of the first laser beam, portions of the steel plate and the Cu interlayer were simultaneously melted, after which the liquid steel and liquid Cu mixed, forming an Fe-rich liquid. Upon cooling, the Fe-rich liquid solidified to form an austenitic region (zone A). Upon further cooling, a Cu-rich phase preferentially precipitated at both the austenitic grain boundaries and the defect sites within the austenitic grains because the solid solubility of Cu in austenite decreases as the temperature decreases according to the binary Fe-Cu phase diagram given by Massalski et al.

[13].

An interfacial reaction layer formed at the zone A-zone B interface, as shown in Fig. 2e. Fig. 2f presents a composite-like structure embedded with coarse globules for the interfacial reaction layer. The EDS analyses indicated that the coarse globules were a Cu-rich phase (areas 8 and 9 in Table 1 and Fig. 2f), and the composite-like structure was characterized by two phases, one being Fe_2Nb (areas 10-12 in Table 1 and Fig. 2g) and the other being the γ matrix (areas 13 and 14 in Table 1 and Fig. 2g). Note that the EDS analyses of Fe_2Nb reflected a low Nb content since the phase was so thin that the γ background was also measured. Furthermore, the EDS analyses confirmed that the fine particles in the γ matrix were Fe_2Nb (areas 15 and 16 in Table 1 and Fig. 2g). The formation of Fe_2Nb indicates that the mutual diffusion of Fe and Nb atoms had already occurred during welding. Fig. 2h and i shows micrographs of zone B. The EDS analyses confirmed that the dark phase was a Cu-rich phase (areas 17 and 18 in Table 1 and Fig. 2h), while gray phase was Fe_7Nb_6 (areas 19-21 in Table 1 and Fig. 2i), and the bright phase was a Nb-rich phase (areas 22-24 in Table 1 and Fig. 2i). Note that the EDS analyses of Fe_7Nb_6 reflected a high Cu content since the Cu-rich phase (areas 25-27 in Table 1 and Fig. 2i) between the Fe_7Nb_6 was also measured. A similar microstructure was observed at the zone B-Nb interface (Fig. 2j). The EDS analyses identified the formation of three phases: a Cu-rich phase (areas 28 and 29 in Table 1 and Fig. 2j), a Nb-rich phase (areas 30-32 in Table 1 and Fig. 2j), and Fe_7Nb_6 (areas 33-35 in Table 1 and Fig. 2j). Because the 1-mm-thick Cu interlayer was incredibly thin, the irradiation of the second laser beam not only melted the remaining Cu interlayer and part of the Nb plate but also remelted part of the austenitic region (which was formed by the irradiation of the first laser beam). An Fe-rich liquid with some Nb and Cu formed at the interface between zone A and zone B. This phenomenon can be ascribed to the lack of mixing of the liquid steel with the bulk of the fusion zone at the zone A-zone B interface due to the rapid heating and cooling rates of laser welding [18]. On the other hand, additional Fe atoms mixed thoroughly with the

Nb atoms in zone B via convection currents and the Marangoni effect [19]. Upon cooling, a mixture of Fe_2Nb lamellae in a γ matrix formed at the zone A-zone B interface [9]. Upon further cooling, fine Fe_2Nb particles precipitated from the γ matrix since the solid solubility of Nb in the γ matrix decreases as the temperature decreases, as indicated in Fig. 3. Additionally, coarse Cu-rich globules precipitated from the Cu-rich liquid. In zone B, however, a eutectic reaction occurred, as indicated by the Nb-rich portion of the Fe-Nb phase diagram (Fig. 3), producing a mixture of Nb and Fe_7Nb_6 [10]. Upon further cooling, a Cu-rich matrix phase precipitated from the Cu-rich liquid. The 1-mm-thick Cu interlayer was clearly too thin to prevent the mutual diffusion of Fe and Nb atoms during laser welding. Therefore, brittle Fe_2Nb and Fe_7Nb_6 formed in the weld.

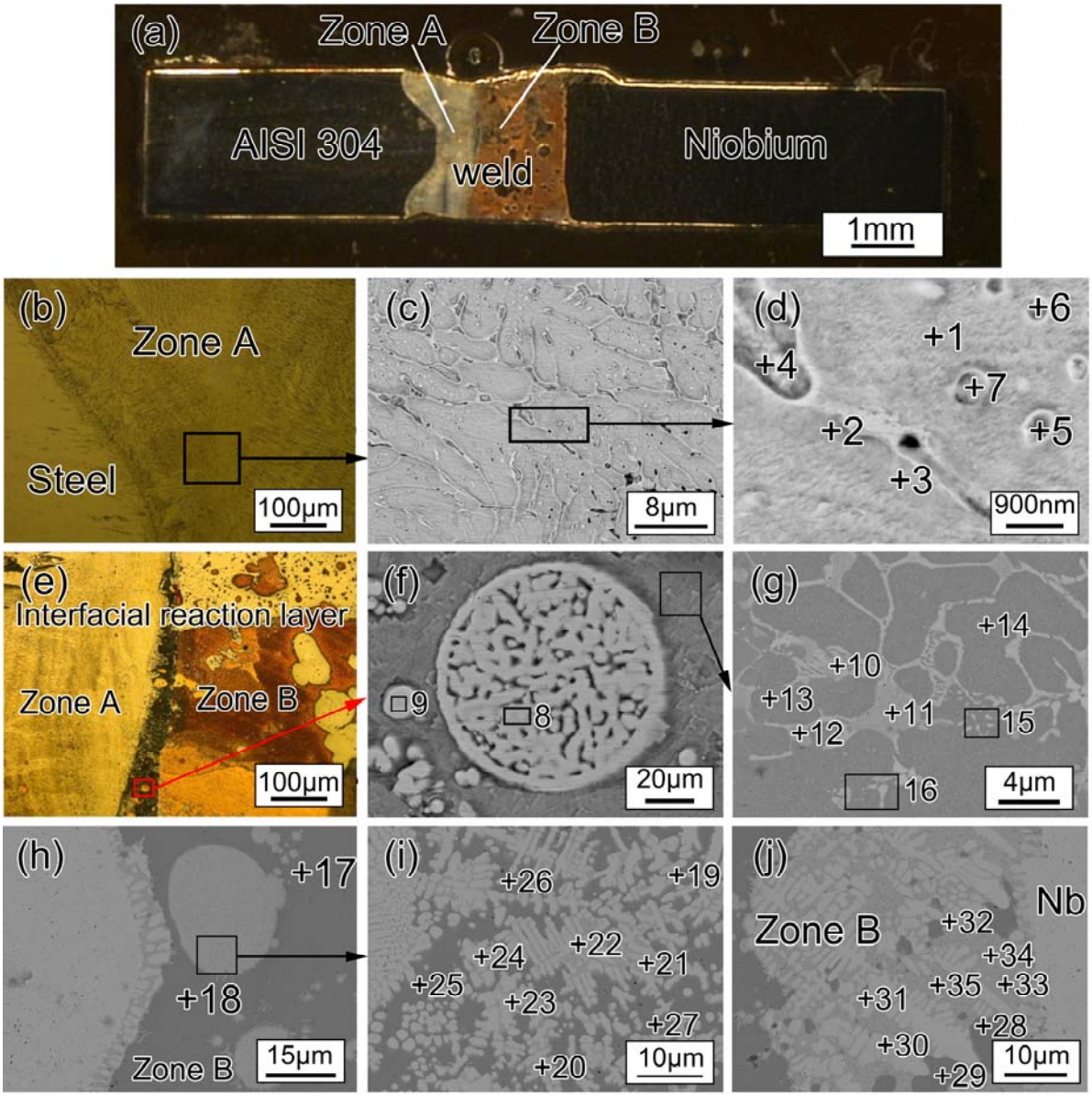

Fig. 2. Microstructure of the joint welded with a 1-mm-thick Cu interlayer. (a) Optical cross-sectional macrograph of the joint. (b) Optical micrograph across the steel-zone A interface. (c) and (d) SEM micrographs of zone A. (e) Optical micrograph across the zone A-zone B interface. (f) and (g) SEM micrographs of the interfacial reaction layer. (h) and (i) SEM micrographs of zone B. (j) SEM micrograph across the zone B-Nb interface.

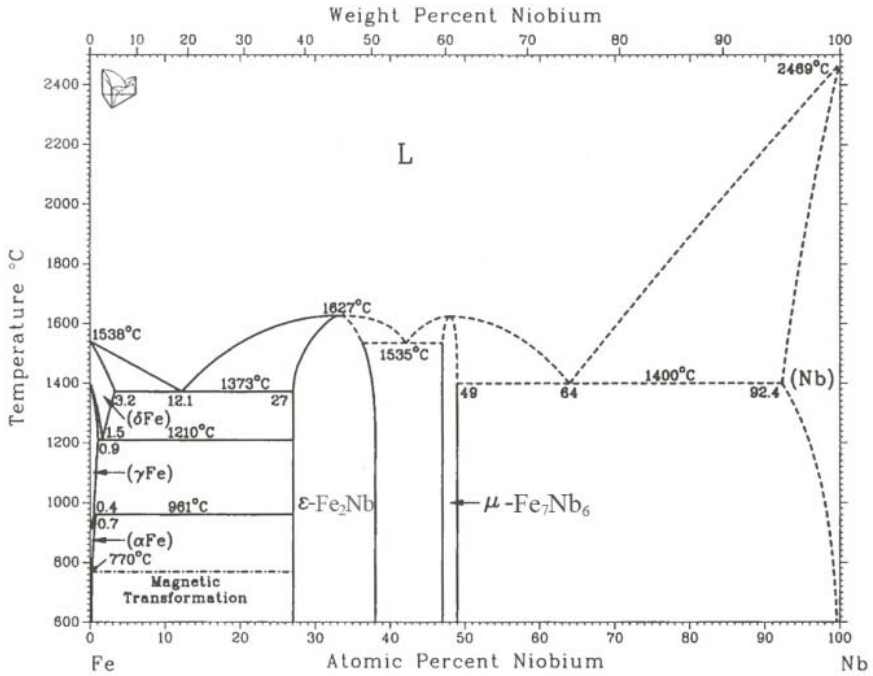

Fig. 3. Binary Fe-Nb phase diagram [13].

Table 1
Chemical compositions of the different phases of the joint welded with a 1-mm-thick Cu interlayer (at.%).

Area	Fe	Cu	Cr	Ni	Nb	Mn	Potential phase
1	66.7	11.6	15.6	6.1	—	—	γ
2	66.6	11.5	16.2	5.7	—	—	γ
3	66.2	11.9	15.9	6	—	—	γ
4	4.1	92.3	1	—	—	2.6	Cu-rich phase
5	5.9	90.2	1.4	—	—	2.5	Cu-rich phase
6	6	90.4	1.4	—	—	2.2	Cu-rich phase
7	6	91	1.2	—	—	1.8	Cu-rich phase
8	—	100	—	—	—	—	Cu
9	3.8	95	1.2	—	—	—	Cu-rich phase
10	62.1	—	13.5	5.7	18.7	—	Fe_2Nb
11	58.7	7.2	12	4.6	17.5	—	Fe_2Nb
12	56	10.5	12.4	4.7	16.4	—	Fe_2Nb
13	69.6	7.3	17.7	5	0.4	—	γ
14	70.7	6.4	17.3	5	0.6	—	γ
15	67.7	5.1	16.8	4.8	5.6	—	γ/Fe_2Nb
16	66	9.5	16.4	4.5	3.6	—	γ/Fe_2Nb
17	1.5	98.5	—	—	—	—	Cu-rich phase
18	—	100	—	—	—	—	Cu
19	28.5	14.4	4.7	—	52.4	—	Fe_7Nb_6
20	22.9	18.2	4.2	—	54.7	—	Fe_7Nb_6
21	29.2	18.8	4.4	—	47.6	—	Fe_7Nb_6
22	5.2	2.2	1.8	—	90.8	—	Nb-rich phase
23	5.1	2.1	1.7	—	91.1	—	Nb-rich phase
24	5	2	1.8	—	91.2	—	Nb-rich phase
25	—	100	—	—	—	—	Cu
26	—	100	—	—	—	—	Cu
27	—	100	—	—	—	—	Cu

28	—	100	—	—	—	—	Cu
29	—	99.9	—	—	0.1	—	Cu-rich phase
30	2.7	2.4	0.9	—	94	—	Nb-rich phase
31	3.3	3	—	—	93.7	—	Nb-rich phase
32	4.8	2.3	1.8	—	91.1	—	Nb-rich phase
33	29.8	15.9	4.6	—	49.7	—	Fe_7Nb_6
34	30.2	17.6	5.3	—	46.9	—	Fe_7Nb_6
35	29.9	17.3	5.2	—	47.6	—	Fe_7Nb_6

3.1.2. Joint with a 1.5-mm-thick Cu interlayer

A cross-sectional macrograph of the joint is shown in Fig. 4a. The macroscopic shape of the joint is similar to that of the joint welded with a 1-mm-thick Cu interlayer. Two distinct regions of the weld were also separately labeled zones A and B.

Fig. 4b-d shows micrographs of zone A. EDS analyses were carried out on the different phases of the joint, and the results are shown in Table 2. The EDS analyses confirmed that the microstructure of zone A consisted of elongated austenitic grains containing some Cu (areas 1-3 in Fig. 4d and Table 2) and Cu-rich precipitates along the austenitic grain boundaries (area 4 in Table 2 and Fig. 4d). These findings are in accordance with the previous microstructural observations from the joint welded with a 1-mm-thick Cu interlayer.

Fig. 4e and f displays micrographs of zone B. The EDS analyses revealed that the Cu matrix in zone B close to zone A contained approximately 3.5 at.% Fe (area 5 in Table 2 and Fig. 4f). In addition, a Cu matrix (areas 6 and 7 in Table 2 and Fig. 4f) embedded with dispersed Nb-rich particles (areas 8-10 in Table 2 and Fig. 4f) was also observed. Note that the EDS analyses of the dispersed Nb-rich particles reflected a high Cu content since the phase was so thin that the Cu background area was also measured. The same phases at the zone B-Nb interface, i.e., a Cu matrix (areas 11 and 12 in Table 2 and Fig. 4g) embedded with Nb-rich dendrites (areas 13 and 14 in Table 2 and Fig. 4g), were identified by the EDS analyses. The irradiation of the second laser beam melted the remaining Cu interlayer and part of the Nb plate. During solidification, the proeutectic Nb first precipitated from the liquid because the eutectic composition of the Cu-Nb eutectic system contained only 0.2 at.% Nb, as

indicated in the binary Cu-Nb phase diagram [13], so the liquid was virtually a hypereutectic liquid. When the temperature was reduced to the eutectic temperature, although all of the remaining liquid underwent a eutectic reaction and transformed into a mixture of Cu and Nb, the amount of Nb in the mixture was almost negligible owing to the extremely low Nb content in the remaining liquid (0.2 at.% Nb). Thus, a two-phase microstructure formed, which was characterized by Nb-rich particles and dendrites embedded in a Cu matrix. In addition, a small amount of Fe dissolved in the Cu matrix in the vicinity of the zone A-zone B interface during the irradiation of the second laser beam. Obviously, the 1.5-mm-thick Cu interlayer prevented the mutual diffusion of Fe and Nb atoms. Therefore, Fe-Nb intermetallic compounds could not form in the weld, and the weld microstructure was composed entirely of solid solution, making it possible to improve the joint strength.

Table 2
Chemical compositions of the different phases of the joint welded with a 1.5-mm-thick Cu interlayer (at.%).

Area	Fe	Cu	Cr	Ni	Nb	Potential phase
1	69.3	5.9	15.6	9.2	—	γ
2	69.1	5.8	15.4	9.7	—	γ
3	69.9	6.3	15	8.8	—	γ
4	10.7	81.1	3.5	4.7	—	Cu-rich phase
5	3.5	95.5	1	—	—	Cu-rich phase
6	—	100	—	—	—	Cu
7	—	100	—	—	—	Cu
8	—	17.9	—	—	82.1	Nb-rich phase
9	—	18	—	—	82	Nb-rich phase
10	—	15.8	—	—	84.2	Nb-rich phase
11	—	100	—	—	—	Cu
12	—	100	—	—	—	Cu
13	—	3.6	—	—	96.4	Nb-rich phase
14	—	5.2	—	—	94.8	Nb-rich phase

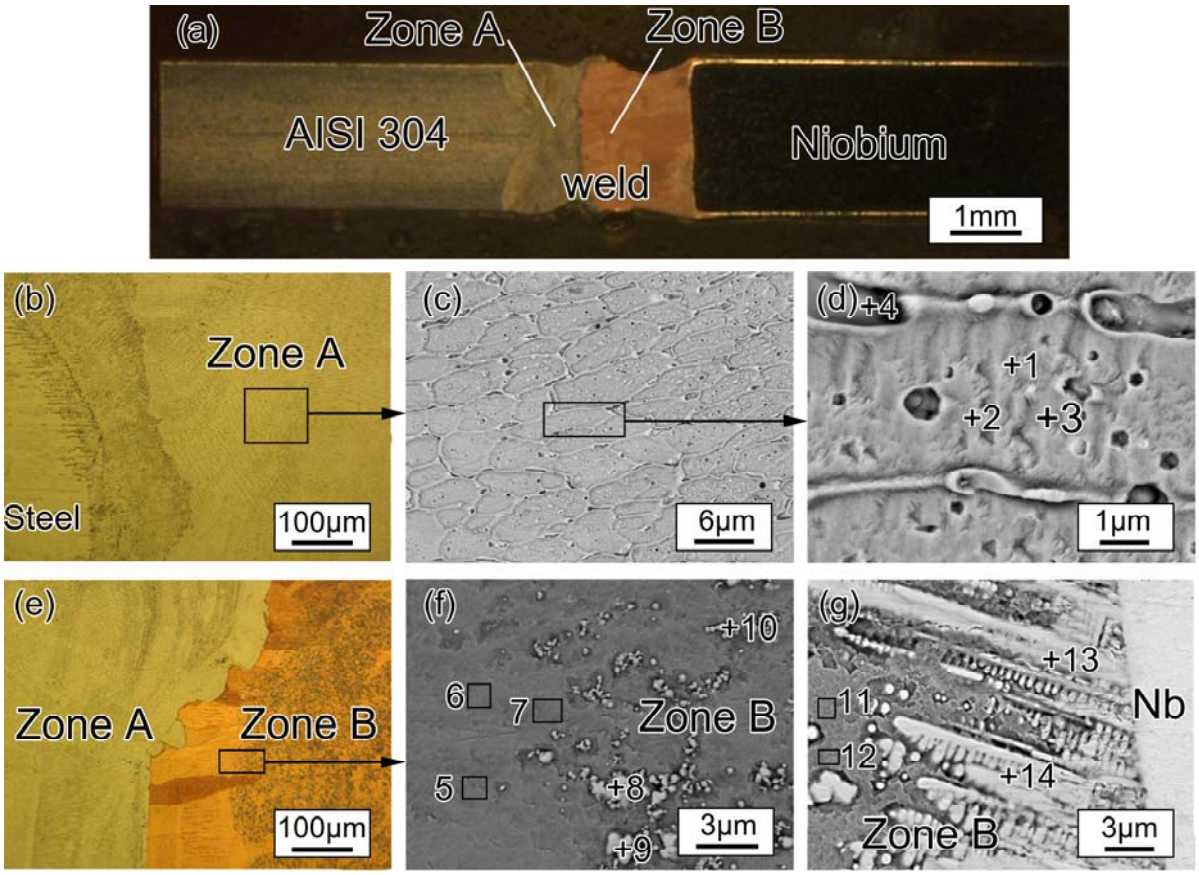

Fig. 4. Microstructure of the joint welded with a 1.5-mm-thick Cu interlayer. (a) Optical cross-sectional macrograph of the joint. (b) Optical micrograph across the steel-zone A interface. (c) and (d) SEM micrographs of zone A. (e) Optical micrograph across the zone A-zone B interface. (f) SEM micrograph of zone B. (g) SEM micrograph across the zone B-Nb interface.

3.1.3. Joint with a 2-mm-thick Cu interlayer

A cross-sectional macrograph of the joint is shown in Fig. 5a. The most prominent macroscopic feature of this joint is the presence of an unmelted Cu interlayer, which was not observed in the joints welded with 1- or 1.5-mm-thick Cu interlayers. This feature can be ascribed to the excessive thickness of the Cu interlayer. Thus, three distinct regions were present in the weld, which are called zone A, the unmelted Cu interlayer, and zone B.

Fig. 5b-d shows micrographs of zone A. A large amount of precipitates was observed, as shown in Fig. 5c and d. EDS analyses were performed on the different phases of the joint, and the results are shown in Table 3. The EDS analyses confirmed that the precipitates were a Cu-rich phase (areas 1-3 in Table 3 and Fig. 5d), while the matrix was austenite (areas 4-6 in Table 3 and Fig. 5d). The microstructure was similar to that of the joint welded with a 1-mm-thick Cu interlayer.

Micrographs of the unmelted Cu interlayer are shown in Fig. 5e and f. The EDS analyses confirmed that the microstructure was composed of a Cu phase (areas 7-9 in Table 3 and Fig. 5f). The presence of the unmelted Cu interlayer demonstrates that the Cu interlayer was too thick to be completely melted by laser beam irradiation.

Micrographs of zone B are shown in Fig. 5g and h. The EDS analyses confirmed that the microstructure consisted of a Nb-rich phase (area 10 in Table 3 and Fig. 5h) and a Cu matrix (areas 11 and 12 in Table 3 and Fig. 5h). At the zone B-Nb interface, the same phases, namely, a Cu matrix (areas 13 and 14 in Table 3 and Fig. 5i) embedded with a Nb-rich phase (areas 15-17 in Table 3 and Fig. 5i), were identified by the EDS analyses. A similar microstructure was previously observed in the joint welded with a 1.5-mm-thick Cu interlayer.

Notably, the excessive thickness of the Cu interlayer ensured that some of the Cu remained in the solid state during welding, successfully preventing the mixing of these two base metals. The unmelted Cu interlayer, however, could weaken the mechanical properties of the joint owing to its low strength.

Table 3
Chemical compositions of the different phases of the joint welded with a 2-mm-thick Cu interlayer (at.%).

Area	Fe	Cu	Cr	Ni	Nb	Mn	Potential phase
1	6.9	87.8	2.7	—	—	2.6	Cu-rich phase
2	6.2	89.2	2.4	—	—	2.2	Cu-rich phase
3	6.8	86.2	2.8	—	—	4.2	Cu-rich phase
4	63.5	14.5	16.2	5.8	—	—	γ
5	64.4	13.7	16.3	5.6	—	—	γ
6	63.8	12.6	16.3	5.4	—	1.9	γ
7	—	100	—	—	—	—	Cu
8	—	100	—	—	—	—	Cu
9	—	100	—	—	—	—	Cu
10	—	3.2	—	—	96.8	—	Nb-rich phase
11	—	100	—	—	—	—	Cu
12	—	100	—	—	—	—	Cu
13	—	100	—	—	—	—	Cu
14	—	100	—	—	—	—	Cu
15	—	3	—	—	97	—	Nb-rich phase
16	—	3	—	—	97	—	Nb-rich phase
17	—	5.4	—	—	94.6	—	Nb-rich phase

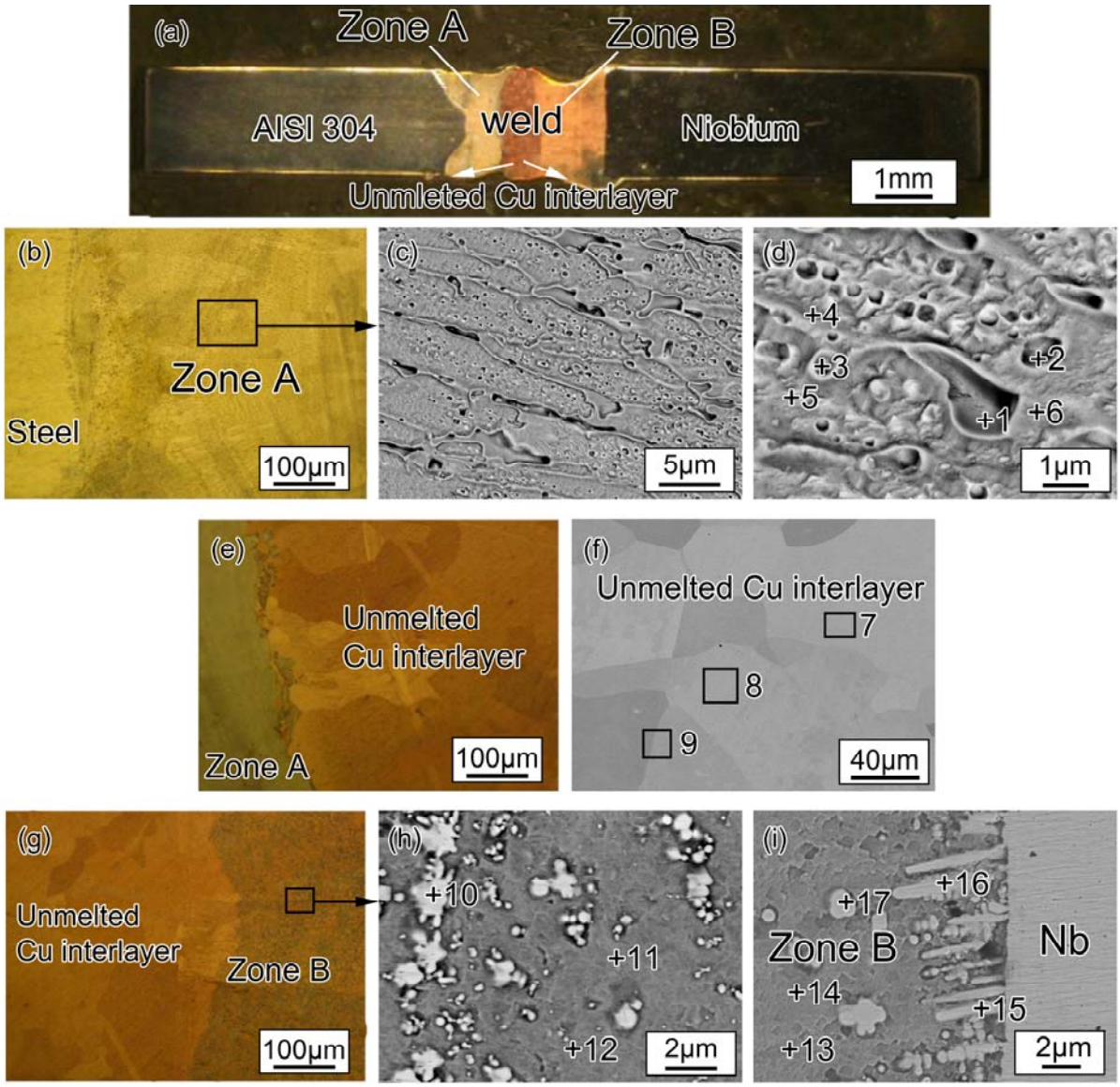

Fig. 5. Microstructure of the joint welded with a 2-mm-thick Cu interlayer. (a) Optical cross-sectional macrograph of the joint. (b) Optical micrograph across the steel-zone A interface. (c) and (d) SEM micrographs of zone A. (e) Optical micrograph across the zone A-unmelted Cu interlayer interface. (f) SEM micrograph of the unmelted Cu interlayer. (g) Optical micrograph across the unmelted Cu interlayer-zone B interface. (h) SEM micrograph of zone B. (i) SEM micrograph across the zone B-Nb interface.

As mentioned above, the most pronounced microstructural feature of the joint with a 1-mm-thick Cu interlayer was the presence of the austenite-Fe_2Nb eutectic and the bulk Fe_7Nb_6, whereas the unmelted Cu interlayer remained in the joint with a 2-mm-thick Cu interlayer. For the joint with a 1.5-mm-thick Cu interlayer, the Fe-Nb intermetallics and unmelted Cu interlayer were totally absent from the weld, which consisted entirely of solid solution.

3.2. Mechanical behavior of the joints

Fig. 6 shows the typical results of the tensile tests. Fracturing occurred in the Nb base metal when using a 1.5-mm-thick Cu interlayer, whereas fracturing occurred in the weld when

using a 1- or 2-mm-thick Cu interlayer. These test results indicate that the tensile strength of the joint was greater than that of the Nb base metal when a 1.5-mm-thick Cu interlayer was adopted. The tensile strength of the specimen welded with a 1.5-mm-thick Cu interlayer exceeded that of the Cu, suggesting that the welded joint obtained a higher strength than that of Cu. It is clear that joint strengthening, especially the strengthening of Cu, clearly occurred. As found by Wendt and Wagner [20], Fe is the most effective added solute with respect to the solid-solution strengthening of Cu; thus, extensive solid-solution strengthening of Cu by Fe occurred. On the other hand, the mixture of Nb-rich particles and dendrites in a Cu matrix was also helpful in improving the mechanical strength of the Cu, since the microhardness value of the former was higher than that of the latter, as indicated in Fig. 7. A similar finding was reported by Youssef et al. [21].

The fracture surface of the tensile specimen welded with a 1-mm-thick Cu interlayer exhibited brittle cleavage fracture features, namely, cleavage faces and river patterns (Fig. 8a), whereas the fracture surface of the tensile specimen welded with a 1.5- or 2-mm-thick Cu interlayer had dimples (Fig. 8b and c), indicating a ductile fracture mode. Furthermore, the EDS analysis of the fracture surface of the tensile specimen welded with a 1-mm-thick Cu interlayer confirmed that the bulk Fe_7Nb_6, as shown in area 1 of Fig. 8a, contributed to the brittle failure of the joint. Note that the mixture of γ and Fe_2Nb at the zone A-zone B interface exhibited a relatively high strength due to the effective dispersion strengthening of the γ matrix by the fine Fe_2Nb lamellae [22]. Thus, fracturing could not occur at the interface. Finally, the EDS analysis of the fracture surface of the tensile specimen welded with a 2-mm-thick Cu interlayer revealed that the fracture occurred in the unmelted Cu interlayer, as shown in area 2 of Fig. 8c. This result can be attributed to the low strength of Cu.

Clearly, the Cu interlayer thickness had an important influence on the mechanical properties of the joint. The mechanical properties of the joint were poor when using a 1-mm-thick Cu interlayer because the interlayer was too thin to prevent the mixing of the two base

metals, and thus, a bulk brittle Fe_7Nb_6 phase formed, thereby embrittling the joint. The mechanical properties of the joint were significantly improved (fracturing occurred in the Nb base metal) when the thickness of the Cu interlayer was increased to 1.5 mm. The reasons for this improvement in mechanical properties can be ascribed to three aspects. First, the 1.5-mm-thick Cu interlayer stopped the mixing of Fe and Nb, thereby inhibiting the formation of Fe-Nb intermetallics. Second, the solid-solution strengthening of Cu by Fe played an important role in improving the mechanical properties of the joint. Third, the mixture of Nb-rich particles and dendrites in the Cu matrix was also beneficial in enhancing the joint strength. However, the mechanical properties of the joint decreased when the thickness of the Cu interlayer was further increased to 2 mm, since the interlayer was too thick to totally melt during laser beam irradiation, and thus, the unmelted Cu interlayer with low strength remained within the weld, causing the joint to fracture in the unmelted Cu interlayer.

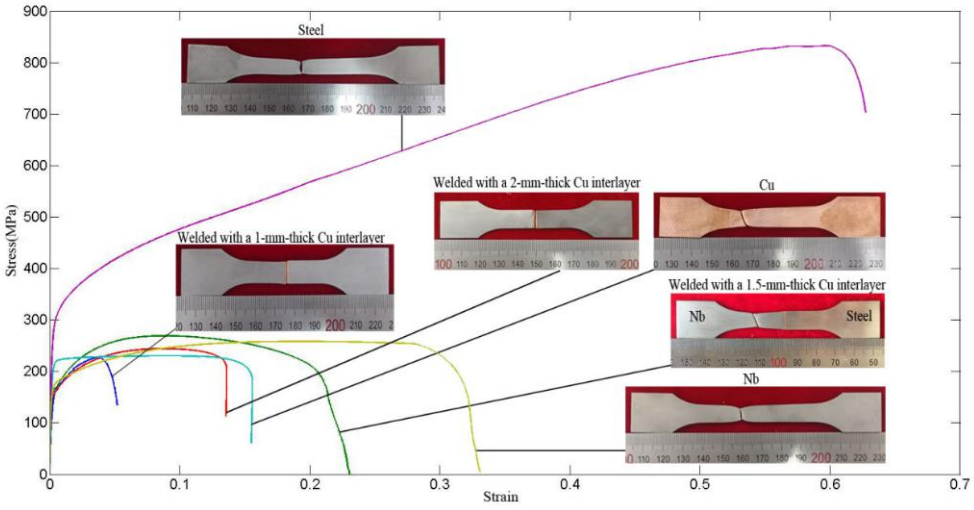

Fig. 6. Typical results of the tensile tests.

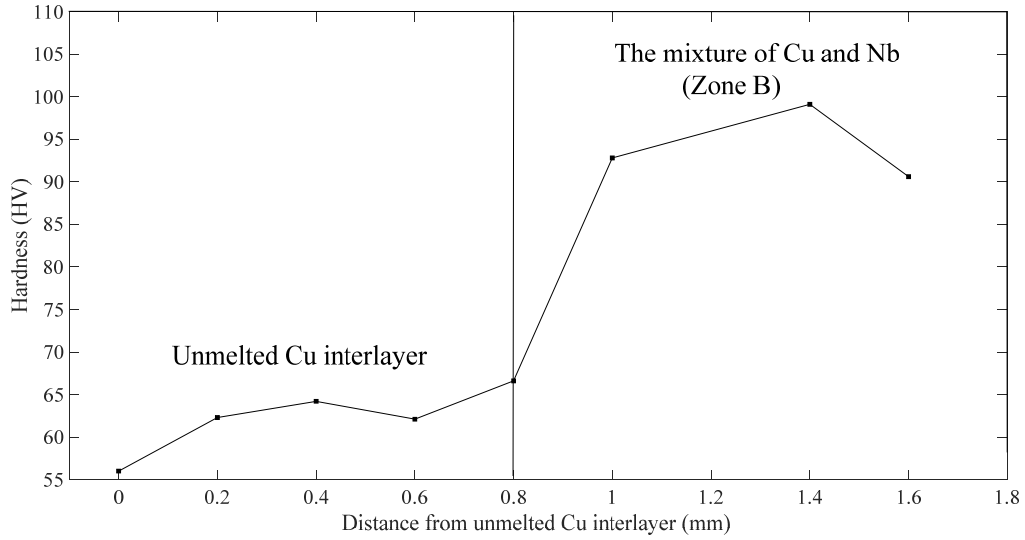

Fig. 7. Microhardness profile of the joint with a 2-mm-thick Cu interlayer.

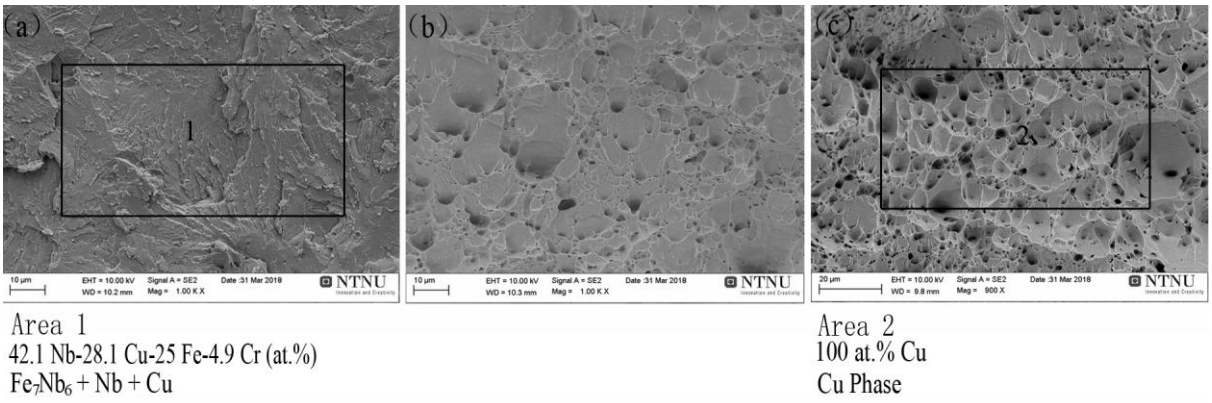

Fig. 8. Fracture surfaces of the tensile specimens welded with (a) a 1-mm-thick Cu interlayer, (b) a 1.5-mm-thick Cu interlayer, and (c) a 2-mm-thick Cu interlayer.

4. Conclusions

Defect-free, dissimilar laser welding of Nb to AISI 304 steel was achieved using a proper Cu interlayer. This achievement opens up the possibility to join these materials in more complex configurations. The following are the major conclusions that can be drawn from this study.

(1) Cu acted as a barrier to mixing between the two base metals, which prevented the formation of brittle intermetallics while ensuring joining between the AISI 304 steel and Nb.

(2) When the thickness of the Cu interlayer was 1 mm, the welded specimen fractured in the weld. The weld microstructure consisted of austenite with Cu-rich particles along the austenitic grain boundaries and within the austenitic grains, a composite-like structure (the

Fe_2Nb lamellae and particles in a γ matrix) embedded with coarse Cu globules, and a mixture of bulk Fe_7Nb_6, Nb-rich dendrites, and Cu matrix. The bulk brittle Fe_7Nb_6 phase embrittled the joint.

(3) When the thickness of the Cu interlayer was 1.5 mm, the welded specimen fractured in the Nb base metal. The weld microstructure consisted of austenite with Cu-rich precipitates along the austenitic grain boundaries and a Cu-rich phase embedded with Nb-rich particles and dendrites. The solid-solution strengthening of Cu by Fe played an important role in improving the mechanical properties of the joint. Moreover, the mixture of Nb-rich particles and dendrites in the Cu matrix was also beneficial in enhancing the joint strength.

(4) When the thickness of the Cu interlayer was 2 mm, the welded specimen also fractured in the weld. The weld microstructure consisted of austenite with Cu-rich precipitates along the austenitic grain boundaries and within the austenitic grains, an unmelted Cu interlayer, and Nb-rich particles and dendrites embedded in a Cu matrix. The unmelted Cu interlayer reduced the joint strength.

Acknowledgments

The authors would like to thank the National Natural Science Foundation of China (Nos. 51605205, 51675248, and 51905332) and the Natural Science Foundation of the Jiangsu Higher Education Institutions of China (No. 15KJB460009) for their support.

References

[1] Kumar A, Ganesh P, Kaul R, et al. Process development for vacuum brazed niobium–316L stainless steel transition joints for superconducting cavities. J Man Sci Eng 2017; 139: 1-8.

[2] Fuerst JD, Toter WF, Shepard KW. Niobium to stainless steel braze transition development. 11th Workshop on RF Superconductivity Conference, 2003: 305-7.

[3] Baghjari SH, Ghaini FM, Shahverdi HR, Mapelli C, Barella S, Ripamonti D. Laser welding of niobium to 410 steel with a nickel interlayer produced by electro spark deposition. Mater Des 2016; 107: 108-16.

[4] Jiao YG, Ma DK, Guo YX, Pei DR. Producing Nb-stainless steel clad rods by outer-clad explosive welding method. Explo Shock Waves 2004; 24(2): 189-92.

[5] Taran Y, Balagurov AM, Sabirov B, Davydov V, Venter AM, Neutron diffraction investigation of residual stresses induced in niobium-steel bilayer pipe manufactured by explosive welding. Mater Sci Forum 2014; 768: 697-704.

[6] Budkin YV, Sokolov YA. A target-oriented method of producing the required temperature field in the weld zone of dissimilar materials. Weld Int 2012; 26(4): 297-302.

[7] Li X, Zheng JP, Zhao J. Characteristics of welding-brazed joint between Nb-1Zr alloy and 304 stainless steel. Trans China Weld Inst 2011; 32(3): 105-8.

[8] Qi LJ, Cai HT. Study on procedure of high-temperature vacuum brazing of Nb-1Zr alloy and 1Cr18Ni9Ti stainless steel. Atom Energy Sci Technol 2007; z1: 365-9.

[9] Hajitabar A, Naffakh-Moosavy H. Electron beam welding of difficult-to-weld austenitic stainless steel/Nb-based alloy dissimilar joints without interlayer. Vac 2017;146: 170–8.

[10] Hajitabar A, Naffakh-Moosavy H. The effect of Fe_xNb_y (x = 2,7 and y = 1,6) intermetallics on microstructure and mechanical properties of electron beam welded Nb-1Zr refractory alloy. Int J Refract Met Hard Mater 2018; 76: 192-203.

[11] Kang Y, Zhan XH, Liu T. Effect of welding parameters on porosity distribution of dual laser beam bilateral synchronous welding in 2219 aluminum alloy T-joint. J Adhes Sci Technol 2019; 33(23): 2595-614.

[12] Shi MX, Zhao J, Hu QX, et al. Influence of the parameters of welding procedure on the mechanical properties of laser welded 304 SS/Nb joint. Trans China Weld Inst 2017; 38(4): 72-6.

[13] Massalski TB, Murray JL, Bennett LH, et al. Binary alloy phase diagrams. American society for metals; 1986.

[14] Shi MX, Li YJ, Ma X. Cu interlayer-induced high-strength laser-welded AISI 304 steel-niobium joint. J Mater Eng Perform 2019; 28(9): 5369-75.

[15] Han DW, Zhang JX. Preparation and display technologies of metallographic samples. Press of central south university; 2005.

[16] Torkamany MJ, Malek Ghaini F, Poursalehi R. Dissimilar pulsed Nd:YAG laser welding of pure niobium to Ti − 6Al − 4V. Mater Des 2014; 53: 915-20.

[17] Magnabosco I, Ferro P, Bonollo F, et al. An investigation of fusion zone microstructures in electron beam welding of copper–stainless steel. Mater Sci Eng A 2006; 424(1-2): 163-73.

[18] Kou S. Welding Metallurgy, second ed. Wiley-interscience; 2003.

[19] Mills KC, Keene BJ, Brooks RF, et al. Marangoni effects in welding. Philos Trans R Soc A 1998; 356(1739): 911-25.

[20] Wendt H, Wagner R. Mechanical properties of Cu-Fe alloys in the transition from solid solution to precipitation hardening. Acta Metall 1982; 30(8): 1561-70.

[21] Youssef KM, Abaza MA, Scattergood RO, et al. High strength, ductility, and electrical conductivity of in-situ consolidated nanocrystalline Cu-1%Nb. Mater Sci Eng A 2018; 711: 350-5.

[22] Maruyama K, Yamada N, Sato H. Effects of lamellar spacing on mechanical properties of fully lamellar Ti-39.4 mol% Al alloy. Mater Sci Eng A 2001; 319-321: 360-3.